Int. J. Heat Mass Transfer. Vol. 31, No. 2, pp. 273–284, 1988
Printed in Great Britain

0017–9310/88 $3.00 + 0.00
Pergamon Journals Ltd.

An experimental and theoretical study of transient free-convection flow between horizontal concentric cylinders

A. CASTREJON
Laboratorio de Energia Solar UNAM, Temixco, Morelos 62580, Mexico

and

D. B. SPALDING
Computational Fluid Dynamics Unit, Imperial College, London SW7, U.K.

(*Received* 31 *August* 1987)

Abstract—This paper reports an experimental and numerical investigation of the transient free-convection flow in the annulus between horizontal concentric cylinders, the inner of which is suddenly heated. In the experiments, photographs were taken of successive positions of the plume of a heated fluid. A finite-domain method was used to simulate the phenomena numerically; and an interface-tracking technique was employed so as to facilitate the comparison of experimental and numerical results.

1. INTRODUCTION

1.1. *The problem considered*

NATURAL convection heat transfer within the annulus between two horizontal concentric cylinders has received considerable attention during the past few years. Numerous applications are found in energy-conversion, energy-storage and energy-transmission systems.

Many theoretical and experimental investigations have been carried out; however, although the accurate prediction of free-convection heat transfer between concentric cylinders has been achieved for steady conditions, the knowledge concerning the transient phenomena is still limited. One of the problems in which knowledge about the transient phenomena is required is that of solar-energy collectors, where the source of energy is by nature intermittent.

This paper presents the results of an experimental and numerical investigation concerning the transient free-convection flow arising within the annulus, when the inner cylinder starts to dissipate heat at a constant rate while the outer wall remains isothermal (Fig. 1).

1.2. *Previous work*

A comprehensive literature survey was presented by Khuen and Goldstein [1], up to the date of which only steady-state conditions had been investigated. In this paper, we present a brief review of selected more recent papers, concerned with both steady and unsteady cases.

Custer and Shaughnessy [2] used a power-series method to obtain solutions for low Prandtl numbers under steady conditions. The same method was also used by Singh and Elliot [3] for dealing with slightly stratified fluids at $Pr = 0.7$. Jischke and Farshchi [4] obtained zeroth-order solutions which account for the coupling of five distinct regions inside the flow by using boundary-layer approximations and integral methods. A parametric study of Prandtl number and diameter-ratio effects on the heat transfer coefficient was performed by Khuen and Goldstein [5], who used a finite-difference formulation.

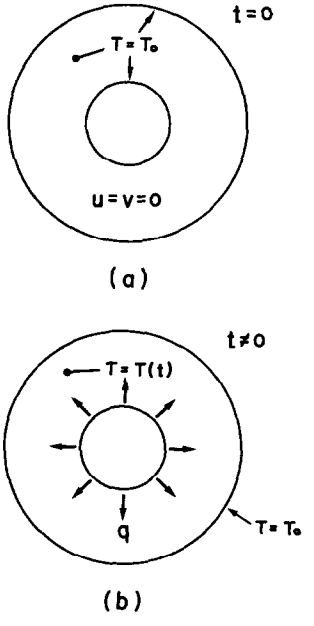

FIG. 1. The situation considered.

NOMENCLATURE

D_i	inner cylinder diameter [m]
F	buoyancy force
g	gravitational acceleration [m s^{-2}]
k	fluid thermal conductivity [W m^{-1} °C^{-1}]
L	gap between outer and inner cylinders [m]
P	pressure [N m^{-2}]
Pr	Prandtl number
q	heat dissipated per unit area [W m^{-2}]
r	radial coordinate [m]
Ra	Rayleigh number
t	time [s]
t^*	dimensionless time
T	temperature [°C]
T^*	dimensionless temperature
$\Delta T'$	modified temperature gradient [°C]
u	tangential velocity component [m s^{-1}]
v	radial velocity component [m s^{-1}].

Greek symbols

α	thermal diffusivity [m^2 s^{-1}]
β	volumetric thermal expansion coefficient [°C^{-1}]
δ_1	maximum distance allowed between particles [m]
δ_2	minimum distance allowed between particles [m]
θ	angular coordinate [rad]
ν	kinematic viscosity [m^2 s^{-1}]
ρ	density [kg m^{-3}]
ψ	stream function [m^2 s^{-1}]
ψ^*	dimensionless stream function.

Subscripts

∞	reference value
i	inner cylinder
o	outer cylinder
old	evaluated at previous time step
p	particle.

The most recent works concerning the steady case are those of Projahn *et al.* [6] who used finite-difference methods to study free convection between concentric and eccentric cylinders; of Castrejon [7] who used a finite-domain formulation to solve the governing equations in terms of the primitive variables; of Takata *et al.* [8] who performed an experimental and theoretical investigation to study the three-dimensional flow which ensues when the symmetry axis is neither horizontal nor perpendicular; of Onyegegbu [9] who used the stream function–vorticity formulation to study the effect of thermal radiation on the free-convection motion; and of Date [10] who used a modified SIMPLE algorithm [11] similar to the one used in this paper to obtain faster convergence.

Concerning the unsteady case, only four works have been reported as far as the present authors are aware. The first one is that of Van de Sande and Hamer [12], who used a simplified mathematical model to predict heat-transfer results, getting good agreement with their own experimental study. Castrejon and Spalding [13] used a finite-domain formulation in dealing with the case of time-dependent temperature on the inner cylinder, the outer remaining at a constant temperature; they obtained numerical flow patterns which were in qualitative agreement with experimental evidence also presented in that work. Tsui and Tremblay [14] solved the problem for two cylinders at constant temperatures through the vorticity–stream function approach by using numerical techniques. Finally, the most recent work on the unsteady phenomena is that of Rao *et al.* [15] who performed a numerical–experimental study to obtain flow patterns by way of streaklines for a wide range of Rayleigh numbers and aspect ratios.

1.3. *The present contribution*

It is the objective of the present work to test the numerical accuracy of a mathematical model and solution procedure capable of predicting the details of free-convection flows. For this purpose, the governing equations are solved by means of the PHOENICS computer code of Spalding [16]; and an interface-tracking technique [17] is attached to it so as to display the flow patterns [18] by means of an imaginary moving interface. While the flow remains laminar, there is little doubt that the numerical technique should, in principle, produce results in accord with experiments; but it may be thought interesting to establish how close an agreement can be achieved with a limited number of grid nodes and time steps.

The predictions are compared with experimental data obtained by means of a flow-visualization technique.

1.4. *Outline of the remainder of the paper*

This paper contains four further sections. Section 2 is concerned with the experimental study. Section 3 presents the governing equations and the assumptions made for their formulation. A statement of the boundary and initial conditions is also given, together with a brief description of the interface-tracking technique and solution method. In Section 4, the mathematical model is applied to the experimental conditions given

in Section 2 and the calculated results are compared with experimental evidence. The final section of the paper summarizes the conclusions.

2. EXPERIMENTAL STUDY

2.1. *Apparatus and experimental procedure*

The apparatus consisted of an electrically-heated inner rod mounted concentrically within an isothermal outer cylinder. The heating element was a carbon rod 0.016 m in diameter and 0.37 m long. The outer cylinder was a 0.27 m long section of a perspex pipe with 0.19 m i.d. and a wall thickness of 0.005 m. Four 0.006 m equally-spaced holes were drilled in the bottom of the apparatus for the valves through which the cavity was filled. An extra 0.003 m hole was drilled in the top so as to act as a pressure relief valve. Two flanges were soldered to each end of the outer cylinder to hold the front and end walls, which had suitably located holes to allow the inner cylinder to pass through. These walls were also made in perspex 0.005 m thick. The apparatus was put together by bolting the end and front walls to the outer cylinder flanges and sealing the carbon rod in the proper position.

Electric power was provided to the carbon rod by means of a variable-current transformer capable of supplying up to 1000 A (a.c.). The fluid used for all the runs was distilled water drawn from a container at laboratory temperature.

To determine the amount of heat dissipated by the inner cylinder, a digital voltmeter (DVM) was connected in parallel with the main-power circuit so as to measure the voltage drop across the carbon rod. The power-input time was measured by means of a simple liquid-crystal display (LCD) clock attached to the apparatus.

The flow patterns arising inside the cavity and the reading of the measuring devices (DVM and clock) were recorded simultaneously by means of still photographs and motion pictures. The camera used to take the still photographs was a Cannon A1 fitted with a 1:1.8 lens and a motor drive; this allowed photographs to be taken at a rate of two frames per second. To improve the contrast between the flow patterns and the background, the cavity was illuminated from behind by a 1000 W IQ photographic lamp with the light passing through a diffuser screen to make the illumination uniform. For a film rated 400 ASA, the exposure was generally set to 1/250 s at f8.0. The motion pictures were obtained by means of a camera and video-cassette recorder. In this case, no extra illumination was required, for the camera is fitted with a light-compensator system which permits the filming to be carried out without any special adjustments. Thus, the entire development of the experimental study was recorded in video-cassettes and the still camera was only used to produce specific results. Figure 2 gives a schematic representation of the complete experimental set-up.

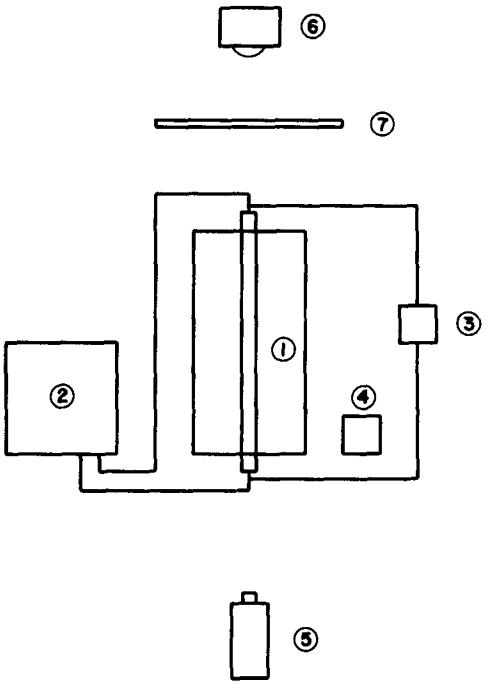

FIG. 2. Schematic representation of the experimental set-up: (1) annular cavity; (2) variable-current transformer; (3) digital voltmeter (DVM); (4) LCD clock; (5) camera; (6) lamp; (7) diffuser screen.

2.2. *Visualization technique*

A review of flow-visualization techniques concerned with heat transfer processes can be found in Merzkirch [19]. However, most of the techniques mentioned in that work have been employed for steady flows and very little attention has been devoted to unsteady free-convection flow visualization. The technique employed in the present research is similar to that used by Stafford [20] and Ilegbusi [21].

This technique consists in the filling of the cavity with two layers of fluid. The layer in the upper-half region of the cavity is pure distilled water of density ρ_1, whereas the lower-half region is a weak salt–dye solution of density ρ_2 (i.e. $\rho_2 > \rho_1$); the concentration of salt is such that the difference of density between the two fluids is large enough to maintain a perfectly horizontal and well-defined interface, yet not so great so as to influence significantly the free-convection flow once the process starts.

At the beginning of each experiment, the front view of the cavity displays a sharp interface separating the dyed solution from the clear water; once the heating process starts, the fluid near the rod heats up and expands until a situation is reached in which the saline solution is less dense at some points than the water in the top (i.e. $\rho_2 < \rho_1$). The motion of the fluid may then be observed by tracing the dye, which is being convected to the clear portion of the cavity. A succession of photographs or a motion picture enables

the various stages of the flow to be recorded for later analysis. Some of the results obtained with the present research are described later in this section.

2.3. *Procedure*

The success of the experiments performed depended to a great extent on the careful filling of the solutions into the cavity, as it was essential to obtain a clear interface between the clear water and the dyed saline solution.

Prior to filling, the cavity was carefully levelled. Then, the clear distilled water was supplied to the cavity until the free-surface touched the inner cylinder; it was then left until any motion of the water had subsided. Next, the dyed saline solution was filled into two four-litre flasks connected to the four holes in the bottom of the cavity via plastic tubes about 0.4 m long; the rate at which the saline solution entered the cavity was controlled by means of tube clamps positioned near the cavity. The saline solution filling process was started by opening the clamps slightly, so as to permit a slow bleed of the solution into the bottom of the cavity; the initial filling rate had to be slow enough to prevent any mixing of the saline solution with the clear water. During the filling process, the flow rate could be increased as the thickness of the saline layer increased; the maximum filling rate was obtained when a small disturbance was observed on the rising interface.

The near-maximum filling rate proved to be essential for a clear interface to be obtained, as a very low filling rate resulted in an interface smeared out by interdiffusion of the two liquid components, and a fast rate resulted in a turbulent mixing process. Typically, it took about 45–50 min to complete the filling process. When the surface of the clear water reached the top of the cavity, the saline solution supply was cut off, leaving the experiment ready to be run.

Running the experiment simply involved starting the clock and the recording system and switching on the transformer to pass the required current through the carbon rod. Because of the density gradient caused by salinity, the motion did not start until the saline solution was hot enough for its density to become smaller than that of the overlying water.

The time required for the motion to start depended on the power input (i.e. heat dissipated); but typically, it took about 10–15 s before the flow could be observed.

2.4. *Experimental results*

Since one of the main objectives of this paper is to provide experimental evidence about the basic flow patterns arising in this kind of flow, the results to be presented here involve the variation of the two adjustable experimental parameters, namely the heat flux and salt concentration. These were chosen so that:

(a) the experiments were long enough to permit the observation of the patterns before the flow became turbulent;

(b) the flow was not significantly affected by the salinity of the solution.

The conditions which were found to be adequate to conform with the two requirements above are:

(a) heat flux: 156 W;
(b) salt concentration: 0.3 g l^{-1}.

Once the heating starts, different flow patterns may be distinguished, namely:

(a) inner boundary layer;
(b) plume;
(c) outer boundary layer.

The first flow pattern occurs when the fluid adjacent to the inner cylinder expands and moves up around it in a boundary layer close to the wall. As the fluid moves up, the thickness of this boundary layer increases until it separates from the wall at the top of the rod. This phenomenon however, cannot be observed with the present experiments because the rod is initially covered by the dyed saline fluid.

The second flow pattern arises when the inner boundary layer separates from the wall at the top of the inner cylinder where a buoyant plume is created; this plume carries the heat absorbed near the inner rod to the upper region of the cavity until it impinges upon the outer wall. Figures 3(a)–(c) show photographs taken of the cavity during the formation of the buoyant plume. The symmetry is excellent.

The fluid then moves in the outer boundary layer along the wall towards the bottom of the cavity. Another interesting feature of the flow emerges at this stage, when the edges of the mushroom-shaped plume become two rolling structures, the centres of rotation of which gradually move towards the outer wall. The photographs given in Figs. 4(a)–(c) display the development of the outer boundary layer and the formation of the vortices described above.

In the last stage of the experiment (Figs. 5(a)–(c)), the outer boundary layer becomes gradually thicker, whilst the rolling structures move back towards the plume. It is also at this time that the first turbulent structures arise in the region adjacent to the outer wall next to the thickest point of the outer boundary layer.

After these patterns are observed, the turbulent structures develop rather rapidly, breaking the symmetry of the flow and hindering any further visual interpretation.

3. MATHEMATICAL MODEL

3.1. *The governing equations*

To obtain a mathematical simulation of the free-convection flow being studied, several assumptions have been made; these may be summarized as follows:

(a) the flow is laminar;

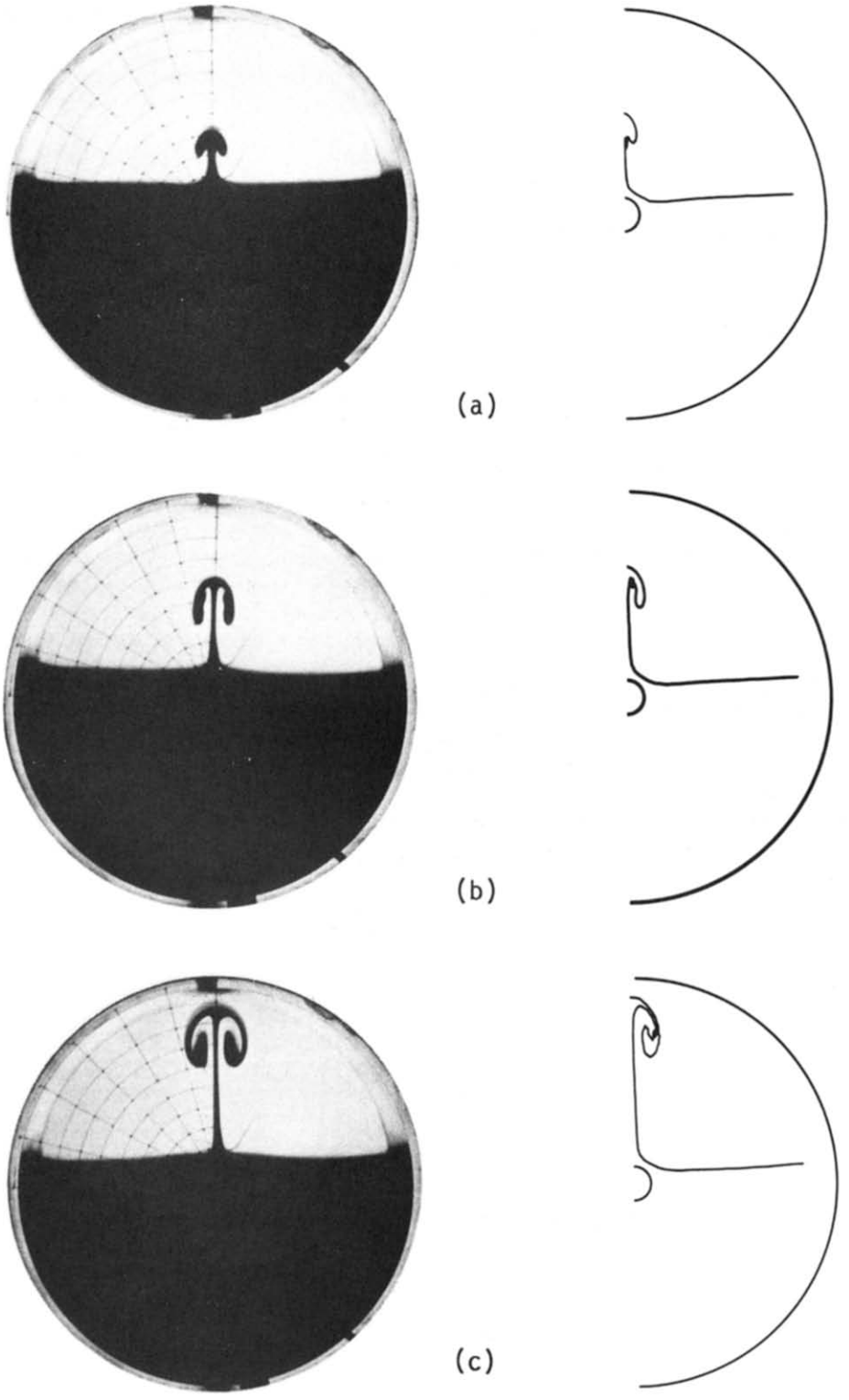

FIG. 3. Comparisons between experimental and numerical flow patterns during the forming-plume stage: (a) $t^* = 2.71 \times 10^{-3}$; (b) $t^* = 3.32 \times 10^{-3}$; (c) $t^* = 4.22 \times 10^{-3}$.

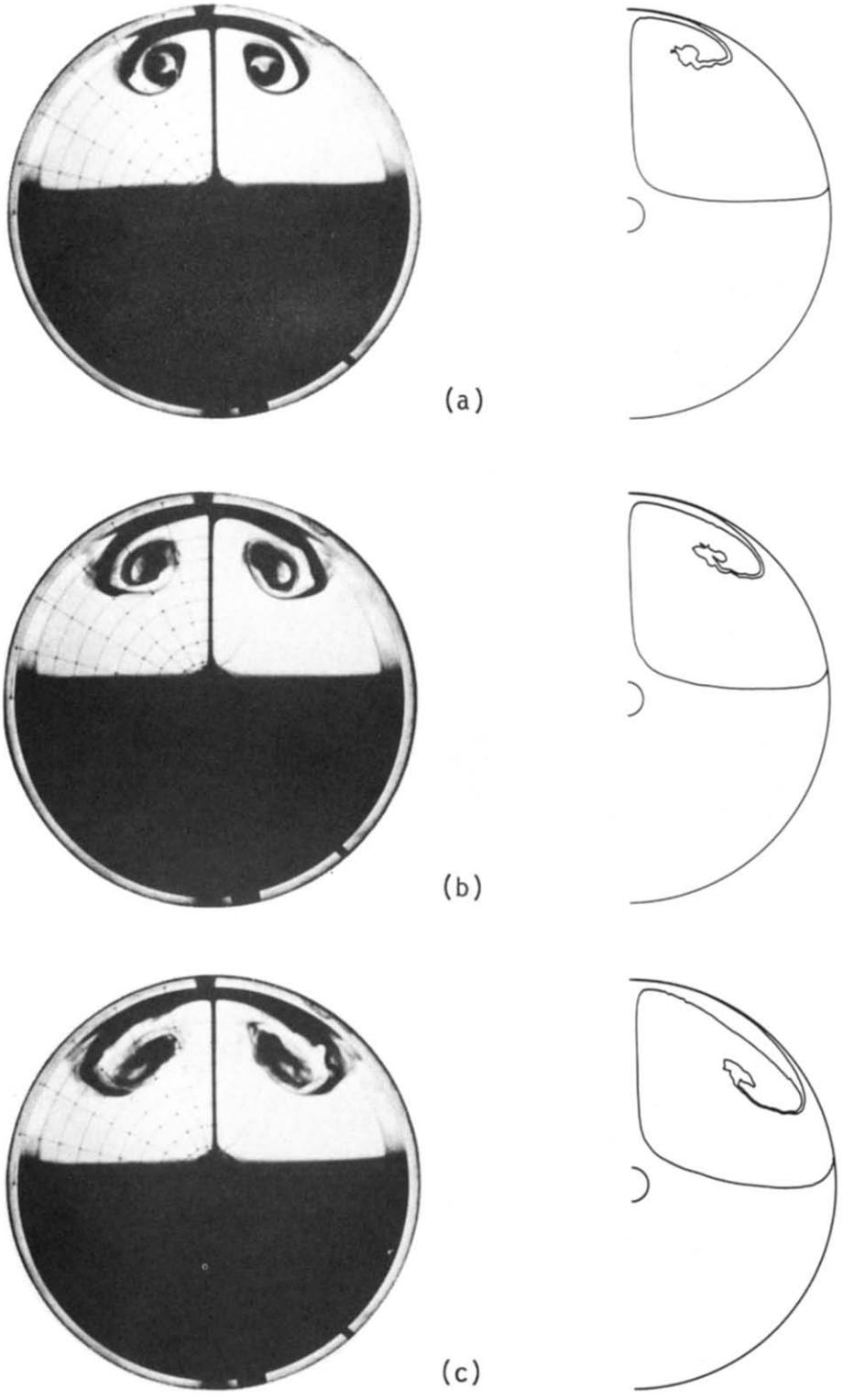

FIG. 4. Comparisons between experimental and numerical flow patterns during the outer-boundary layer stage: (a) $t^* = 6.03 \times 10^{-3}$; (b) $t^* = 6.94 \times 10^{-3}$; (c) $t^* = 7.85 \times 10^{-3}$.

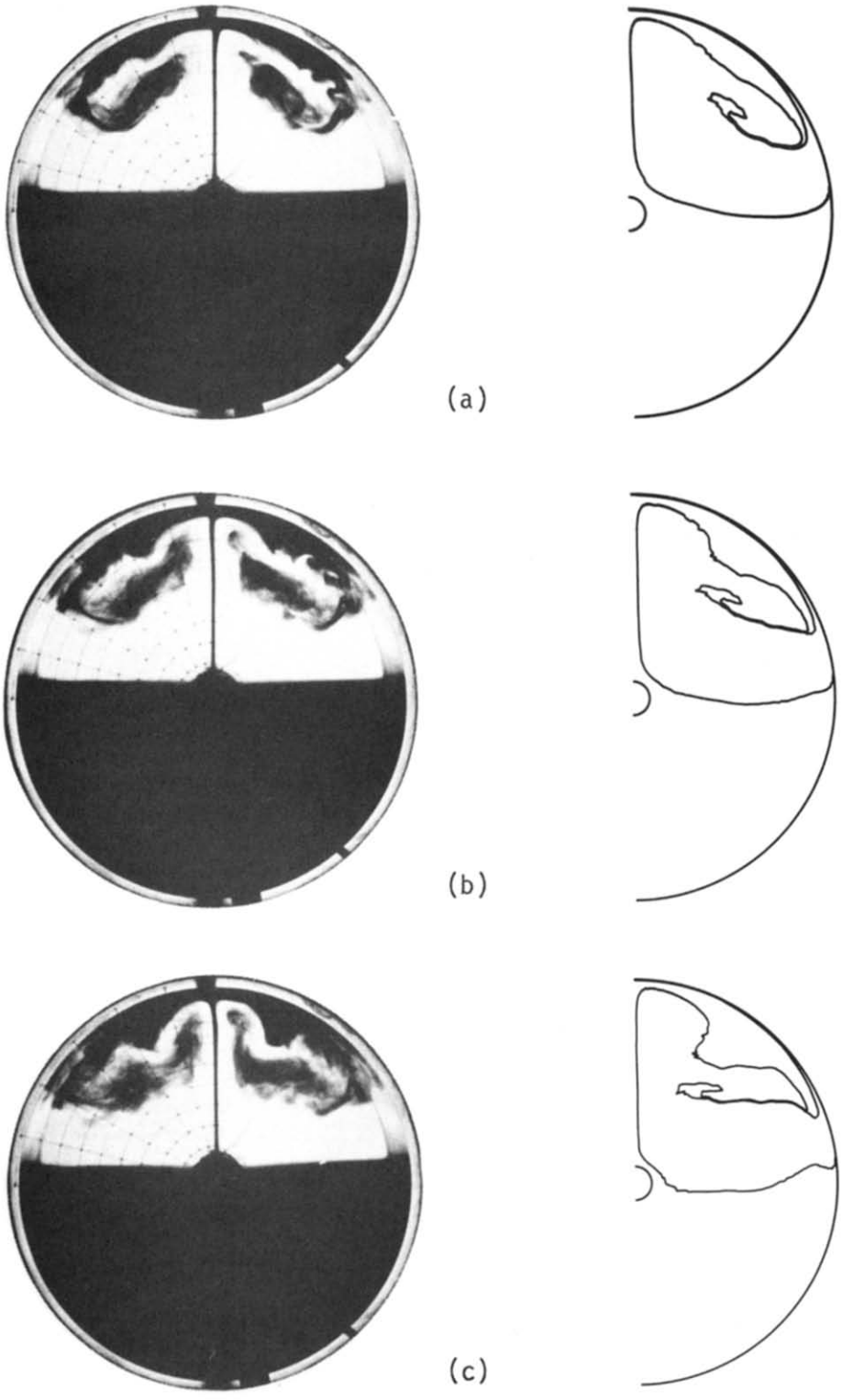

FIG. 5. Comparisons between experimental and numerical flow patterns during the last stage of the process: (a) $t^* = 8.45 \times 10^{-3}$; (b) $t^* = 9.05 \times 10^{-3}$; (c) $t^* = 9.66 \times 10^{-3}$.

(b) the axis of the cylinders is infinite in length, rendering the problem two-dimensional;

(c) the fluid is incompressible and all its properties are constant except that the Boussinesq approximation is used for the density in the buoyancy term of the momentum equation;

(d) viscous dissipation is negligible in the energy equation.

In addition, a vertical plane passing through the centre of the system divides the flow domain in two symmetric halves, so that only one half needs to be studied.

The governing equations corresponding to the above-mentioned assumptions in polar coordinates are given below.

Continuity equation

$$\frac{\partial v}{\partial r}+\frac{v}{r}+\frac{1}{r}\frac{\partial u}{\partial \theta}=0. \tag{1}$$

θ-Component of the momentum equation

$$\frac{\partial u}{\partial t}+v\frac{\partial u}{\partial r}+\frac{u}{r}\frac{\partial u}{\partial \theta}+\frac{uv}{r}=-\frac{1}{\rho r}\frac{\partial P}{\partial \theta}+\nu\left[\frac{\partial}{\partial r}\left(\frac{1}{r}\frac{\partial}{\partial r}(ur)\right)+\frac{1}{r^2}\frac{\partial^2 u}{\partial \theta^2}+\frac{2}{r^2}\frac{\partial v}{\partial \theta}\right]+F_\theta. \tag{2}$$

r-Component of the momentum equation

$$\frac{\partial v}{\partial t}+v\frac{\partial v}{\partial r}+\frac{u}{r}\frac{\partial v}{\partial \theta}-\frac{u^2}{r}=-\frac{1}{\rho}\frac{\partial P}{\partial r}+\nu\left[\frac{\partial}{\partial r}\left(\frac{1}{r}\frac{\partial}{\partial r}(vr)\right)+\frac{1}{r^2}\frac{\partial^2 v}{\partial \theta^2}-\frac{2}{r^2}\frac{\partial u}{\partial \theta}\right]+F_r. \tag{3}$$

Energy equation

$$\frac{\partial T}{\partial t}+v\frac{\partial T}{\partial r}+\frac{u}{r}\frac{\partial T}{\partial \theta}=\alpha\left[\frac{1}{r}\frac{\partial}{\partial r}(r)\frac{\partial T}{\partial r}+\frac{1}{r^2}\frac{\partial^2 T}{\partial \theta^2}\right]. \tag{4}$$

The space coordinates are r, measured from the centre of the system, and θ, measured clockwise from the upward vertical symmetry line. The radial velocity v is positive radially outwards and the angular velocity u is positive in the clockwise direction for $0<\theta<\pi$. In accordance with the Boussinesq approximation, the buoyancy force terms are written as functions of the local temperature difference as

$$F_\theta=\rho_\infty g\beta(T-T_\infty)\sin\theta \tag{5}$$

for the angular direction, and

$$F_r=\rho_\infty g\beta(T-T_\infty)\cos\theta \tag{6}$$

for the radial direction.

To complete the specification of the mathematical formulation, both initial and boundary conditions are needed.

Initial conditions ($t=0$):

(a) $u=v=0$ for all values of r and θ; (7)

(b) $T=T_\infty$ for all values of r and θ. (8)

Boundary conditions ($t>0$):

(a) inner cylinder ($r=r_i$; $0<\theta<\pi$)

$$u=v=0 \tag{9}$$

$$\frac{dT}{dr}=\text{constant}; \tag{10}$$

(b) outer cylinder ($r=r_o$; $0<\theta<\pi$)

$$u=v=0 \tag{11}$$

$$T=T_\infty; \tag{12}$$

(c) symmetry lines ($r_i<r<r_o$; $\theta=0$ and π)

$$\frac{du}{d\theta}=\frac{dT}{d\theta}=0. \tag{13}$$

3.2. *Solution of the equations*

The mathematical model presented in the previous sub-section forms a closed system of four coupled differential equations. These equations have been supplied with the associated initial and boundary conditions and then solved using the elliptic equation, implicit finite-domain solution procedure embodied in the PHOENICS computer code of Spalding [16], and based upon the frequently described Patankar–Spalding method [11].

3.3. *Interface tracking*

The successful calculation of flows with moving interfaces requires a detailed knowledge of the shape and location of the fluid interface. In the present study, the particle-tracking technique used by Maxwell [17] and Awn [22] was incorporated into the PHOENICS code. Its mathematical basis will now be briefly described.

The technique consists in the distributing of a series of imaginary particles at some initial time t_{old} over the interface. Each of these particles is characterized by coordinates θ_p and r_p, where the subscript p denotes the particle. These particles are moved at the end of each time step according to the velocities computed for the flow domain; so, from their new locations, the new shape and position of the interface may be determined at each time step. The variation of each particle position with time is deduced from the following equations:

$$\frac{d\theta_p}{dt}=u_p \tag{14}$$

$$\frac{dr_p}{dt}=v_p \tag{15}$$

which may be written in finite-difference form as

$$\theta_p=\theta_{p,old}+u_p\Delta t \tag{16}$$

$$r_p=r_{p,old}+v_p\Delta t \tag{17}$$

where θ_p and r_p are the new coordinates of the particle and u_p and v_p are the instantaneous velocity components with which the particles are moved through

the flow domain, and which are evaluated at the 'old' location $(\theta_{p,old}, y_{p,old})$.

There are several methods of calculating the particle velocities (see, e.g. Daly [23]). The method chosen here consists of evaluating the particle velocity components by a direct linear interpolation of the neighbouring four velocities surrounding the particle; however, for the particles which lie near the boundaries, the fluid velocities used to calculate the particle velocities all lie in the fluid side [24].

Because of the fluid motion, the particles do not always remain evenly spaced. After some time, parts of the interface may be sparsely populated with particles, while in other sections, the particles may be closely packed; either extreme is bad. Therefore, a check of the space between adjacent particles is the first step in the tracking calculation. If a pair of particles is separated by more than a maximum distance δ_1, a new particle is inserted between them; the coordinates of the new particle are taken to be the average coordinates of its neighbours, and the particle storage array is adjusted to accommodate the new particle. If the space between successive particles is less than a prescribed minimum distance δ_2, one of the particles is deleted and the particle storage array is again modified to maintain an orderly sequence.

3.4. *Computational details*

To keep the convergence time to a minimum without sacrificing accuracy, a non-uniform grid was used so as to accommodate more grid nodes where large gradients of the flow variables were expected. This practice was adopted near the walls in the radial direction and near the upper symmetry line in the angular direction. A grid of 30 intervals in the r-direction and 20 in the θ-direction was fine enough to produce a grid-independent solution.

Tests were also performed with the above-mentioned grid and different sizes of the time step δt. Typically, to obtain a time-step-independent solution, a δt smaller than 0.05 s was required.

The calculations were performed on a Perkin–Elmer 3220 minicomputer. The time required with the basic grid used was about 56 s per time step; and the storage required was 429 Kb.

3.5. *Numerical results*

The dimensionless parameters that govern the flow are:

aspect ratio

$$L/D_i; \tag{18}$$

Prandtl number

$$Pr = \nu/\alpha; \tag{19}$$

Rayleigh number

$$Ra = \frac{g\beta L^3 \Delta T'}{\nu\alpha}; \tag{20}$$

where $\Delta T'$ is a modified temperature difference given by

$$\Delta T' = \frac{r_i q}{k}. \tag{21}$$

The flow patterns are conveniently described in terms of the stream function ψ, defined by way of

$$u = -\frac{\partial \psi}{\partial r} \tag{22}$$

$$v = \frac{1}{r}\frac{\partial \psi}{\partial \theta}. \tag{23}$$

The streamlines and isotherms of the flow are presented in terms of the dimensionless values defined as

$$\psi^* = \frac{\psi}{\nu} \tag{24}$$

and

$$T^* = \frac{(T - T_\infty)}{\Delta T'} \tag{25}$$

as functions of the dimensionless time t^*

$$t^* = \frac{t\nu}{L^2} \tag{26}$$

Figures 6(a)–(d) show the streamlines and isotherms for the flow described in Section 2. The conditions correspond to the following values of the dimensionless parameters:

(a) Prandtl number: 7.0;
(b) Rayleigh number: 6.3×10^8;
(c) aspect ratio: $L/D_i = 5.5$.

From Fig. 6(b) it may be seen that, after the hot fluid impinges upon the outer wall, a radial temperature inversion appears, the fluid near to the outer wall being warmer than that near to the inner cylinder; this is obviously due to the strongly recirculating nature of the flow.

Finally, in Fig. 6(d), it can be seen that a secondary eddy appears just over the level of the inner cylinder. However, this secondary eddy is very weak, as the velocities occurring in that region are small compared with those in the main eddy.

4. COMPARISONS BETWEEN EXPERIMENTAL AND NUMERICAL RESULTS

In Section 2.4 of this paper, a qualitative description was given of the basic flow patterns arising in the flow under consideration. In this section, attention will be given to the accuracy with which the mathematical model predicts this flow.

Figure 3 compares the photographs and predictions of the plume shape and position at three different times. It may be seen in this figure that the agreement between the experimental and numerical flow patterns at this stage is fairly good.

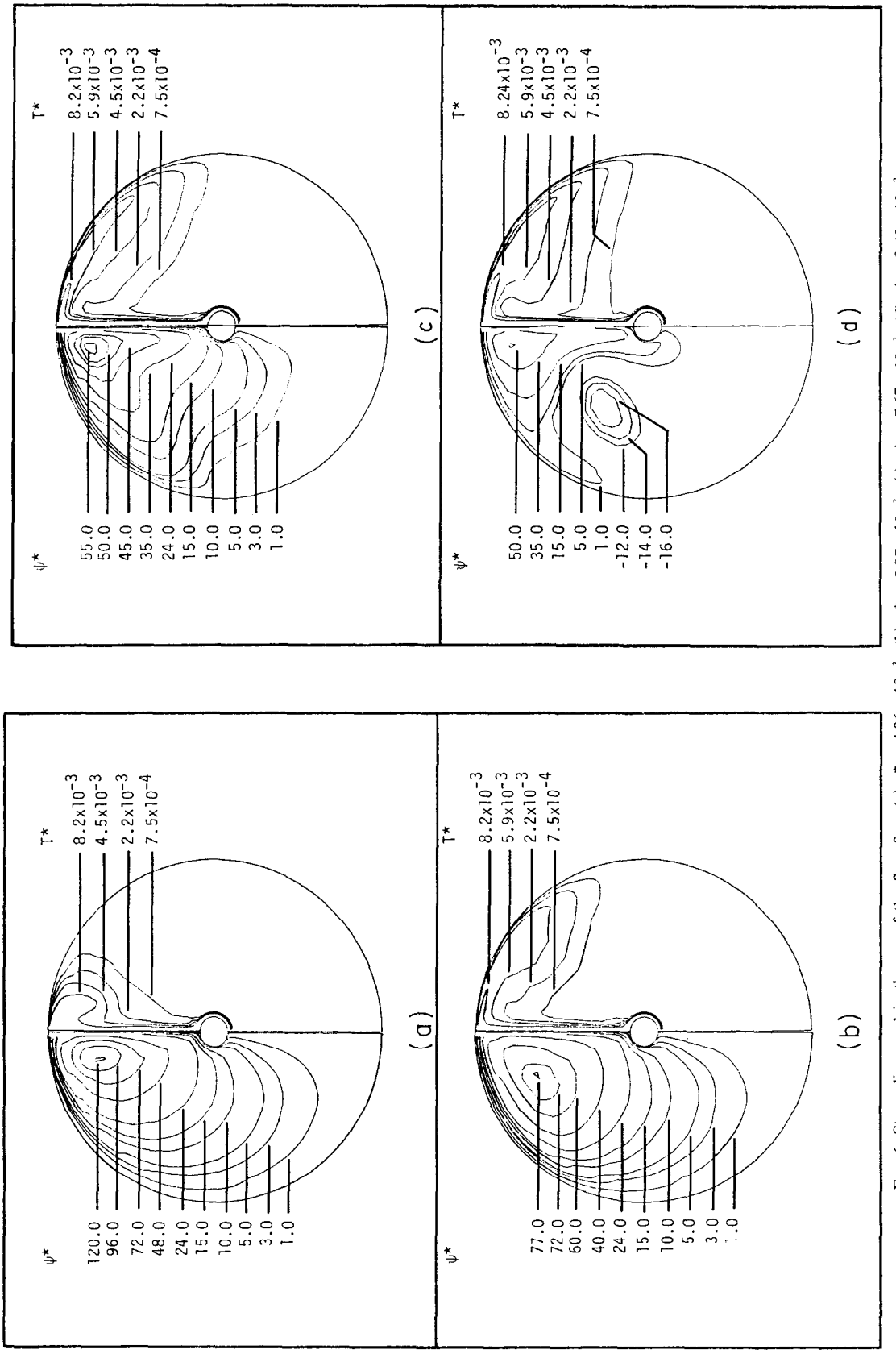

FIG. 6. Streamlines and isotherms of the flow for: (a) $t^* = 4.06 \times 10^{-3}$; (b) $t^* = 5.87 \times 10^{-3}$; (c) $t^* = 7.67 \times 10^{-3}$; (d) $t^* = 9.48 \times 10^{-3}$.

In Fig. 4, comparisons are presented between the experimental and numerical flow patterns occurring during the development of the outer boundary layer. This figure shows that although the model can adequately predict the development of the boundary layer along the outer wall, it does not represent the rate of rotation of the rolling structures properly. This is however less in evidence at later times, when the structures no longer rotate but merely translate, keeping nearly the same orientation; this is well predicted by the model.

Finally, Fig. 5 shows the experimental and numerical flow patterns arising during the last stage of the process. Again, the numerical model performs well in predicting the motion and orientation of the rolling structures; the further development of the outer boundary layer, the rate at which it becomes thicker, and the position and shape of its thickest point, are also well represented.

The major discrepancies between the experimental and numerical results occur during the last stage. In Fig. 5(c) it may be seen that towards the end of the process there is an extra structure, which consists of a portion of fluid rising again parallel to the central plume; this is not predicted by the numerical model. Also, the horizontal portion of fluid just below the thickest point of the outer boundary layer seems to be considerably thicker in the experiment than in the predictions. The reasons for these discrepancies may be that both the observation of the rising fluid and the thickening of the horizontal line are consequences of the diffusion of the dyed fluid into the clear one, whereas the interface-tracking technique employed in this study accounts only for convective motions of the interface and completely disregards diffusive effects.

5. CONCLUDING REMARKS

The numerical solution procedure has afforded considerable insight into both the general patterns and the detailed features of the flow of heat and fluid in the transient-heat-transfer experiment. Moreover, the comparisons of predictions with experiments show fairly good qualitative and quantitative agreement. The numerical model is however, as yet incapable of predicting the transition to random motion which occurs towards the end of the observation period.

Acknowledgements—Thanks are due to Mr F. J. King for his assistance in the experimental and photographic work.

REFERENCES

1. T. H. Khuen and R. J. Goldstein, An experimental and theoretical study of natural convection in the annulus between horizontal concentric cylinders, *J. Fluid Mech.* **74,** 695 (1976).
2. J. R. Custer and E. J. Shaughnessy, Thermoconvective motion of low Prandtl number fluids within a horizontal cylindrical annulus, *J. Heat Transfer* **99,** 596 (1977).
3. S. N. Singh and J. M. Elliot, Free convection between horizontal concentric cylinders in a slightly thermally stratified fluid, *Int. J. Heat Mass Transfer* **22,** 639 (1979).
4. M. C. Jischke and M. Farshchi, Boundary layer regime for laminar free convection between horizontal circular cylinders, *J. Heat Transfer* **102,** 228 (1980).
5. T. H. Khuen and R. J. Goldstein, A parametric study of Prandtl number and diameter ratio effects on natural convection heat transfer in horizontal cylindrical annuli, *J. Heat Transfer* **102,** 768 (1980).
6. U. Projahn, H. Rieger and H. Beer, Numerical analysis of laminar natural convection between concentric and eccentric cylinders, *Numer. Heat Transfer* **4** (1981).
7. A. Castrejon, Natural convection inside an annular cavity, Imperial College of Science and Technology, PDR/CFDU IC/9 (1983).
8. Y. Takata, K. Iwashige, K. Fukuda and S. Hasegawa, Three-dimensional natural convection in an inclined cylindrical annulus, *Int. J. Heat Mass Transfer* **27,** 747 (1984).
9. S. O. Onyegegbu, Heat transfer inside a horizontal cylindrical annulus in the presence of thermal radiation and buoyancy, *Int. J. Heat Mass Transfer* **29,** 659 (1986).
10. A. W. Date, Numerical prediction of natural convection heat transfer in horizontal annulus, *Int. J. Heat Mass Transfer* **29,** 1457 (1986).
11. S. V. Patankar and D. B. Spalding, A calculation procedure for heat mass and momentum transfer in three-dimensional parabolic flows, *Int. J. Heat Mass Transfer* **15,** 1787 (1972).
12. E. Van de Sande and B. J. G. Hamer, Steady and transient natural convection in enclosures between horizontal circular cylinders (constant heat flux), *Int. J. Heat Mass Transfer* **22,** 361 (1979).
13. A. Castrejon and D. B. Spalding, Unsteady laminar natural convection inside an annular cavity, Imperial College of Science and Technology, Report CFD/83/8 (1983).
14. Y. T. Tsui and B. Tremblay, On transient natural convection heat transfer in the annulus between concentric horizontal cylinders with isothermal surfaces, *Int. J. Heat Mass Transfer* **27,** 103 (1984).
15. Y. F. Rao, Y. Miki, K. Fukuda, Y. Takata and S. Hasegawa, Flow patterns of natural convection in horizontal cylindrical annuli, *Int. J. Heat Mass Transfer* **28,** 705 (1985).
16. D. B. Spalding, A general-purpose computer program for multi-dimensional one- and two-phase flow. In *Mathematics and Computers in Simulation*, Vol. XXIII, p. 267. North-Holland, Amsterdam (1981).
17. T. T. Maxwell, Numerical modelling of free-surface flows, Ph.D. Thesis, University of London (1977).
18. A. Castrejon, Particle-tracking subroutines for numerical flow visualisation, Imperial College of Science and Technology, PDR/CFDU IC/10 (1983).
19. W. Merzkirch, Visualization of heat transfer, *Proc. 7th Heat Transfer Conf.*, Vol. 1, p. 91 (1982).
20. L. G. Stafford, An experimental investigation of turbulent mixing due to buoyancy forces in unstable stratified media, Imperial College of Science and Technology, Report CFD/82/10 (1982).
21. J. O. Ilegbusi, A revised two-equation model of turbulence, Ph.D. Thesis, University of London (1983).
22. A. G. Awn, Numerical modelling of flows with moving interfaces, Ph.D. Thesis, University of London (1979).
23. B. J. Daly, A technique for including surface tension effects in hydrodynamic calculations, *J. Computational Phys.* **4,** 97 (1969).
24. A. Castrejon, Unsteady free-convection heat transfer inside an annular cavity, Ph.D. Thesis, University of London (1984).

ETUDE EXPERIMENTALE ET THEORIQUE DE CONVECTION NATURELLE VARIABLE ENTRE CYLINDRES CONCENTRIQUES ET HORIZONTAUX

Résumé—On décrit une recherche expérimentale et numérique sur l'écoulement variable de convection naturelle dans un espace annulaire entre deux cylindres concentriques, horizontaux, le plus petit des deux étant soudainement chauffé. Dans les expériences, des photographies sont prises sur les positions successives du panache de fluide chaud. Une méthode de domaine fini est utilisée pour simuler numériquement les phénomènes, et une technique de poursuite d'interface est utilisée pour faciliter la comparaison des résultats du calcul et de l'expérience.

EXPERIMENTELLE UND THEORETISCHE UNTERSUCHUNG DER INSTATIONÄREN FREIEN KONVEKTION ZWISCHEN WAAGERECHTEN KONZENTRISCHEN ZYLINDERN

Zusammenfassung—In der Arbeit wird über eine experimentelle und numerische Untersuchung der instationären Konvektionsströmung im Ringraum zwischen zwei waagerechten, konzentrisch angeordneten Zylindern berichtet, von denen der innere plötzlich beheizt wird. Während der Versuche wurde die aufgeheizte Strömung zu verschiedenen, aufeinander folgenden Zeitpunkten fotografiert. Mit einer Methode der finiten Bereiche wurde das Phänomen numerisch simuliert. Um Vergleiche zwischen experimentellen und numerischen Ergebnissen anstellen zu können, wurde eine Methode zum Nachfahren der Grenzschicht verwendet.

ЭКСНЕРИМЕНТАЛЬНОЕ И ТЕОРЕТИЧЕСКОЕ ИССЛЕДОВАНИЕ НЕСТАЦИОНАРНОЙ СВОБОДНОЙ КОНВЕКЦИИ МЕЖДУ ГОРИЗОНТАЛЬНЫМИ КОНЦЕНТРИЧЕСКИМИ ЦИЛИНДРАМИ

Аннотация—Экспериментально и численно исследуется нестационарное свободно-конвективное течение в кольцевом зазоре, образованном горизонтальными концентрическими цилиндрами, внутренний из которых мгновенно нагревается. В экспериментах фотографировались последовательные положения восходящего потока нагретой жидкости. Метод конечных элементов использовался для численного моделирования. Проведено сравнение экспериментальных и численных результатов.